Icarus 261 (2015) 169–181

Contents lists available at ScienceDirect

Icarus

journal homepage: www.elsevier.com/locate/icarus

Recent near-surface wind directions inferred from mapping sand ripples on Martian dunes

Zac Yung-Chun Liu [a,b,*], James R. Zimbelman [c]

[a] Department of Geological Sciences, Brigham Young University, Provo, UT 84602, USA
[b] Now at School of Earth and Space Exploration, Arizona State University, Tempe, AZ 85287, USA
[c] Center for Earth and Planetary Studies, National Air and Space Museum, MRC 315, Smithsonian Institution, Washington, DC 20013-7012, USA

ARTICLE INFO

Article history:
Received 21 January 2015
Revised 13 August 2015
Accepted 13 August 2015
Available online 24 August 2015

Keywords:
Aeolian processes
Mars, surface
Geological processes

ABSTRACT

The High Resolution Imaging Science Experiment (HiRISE) provides the capability to obtain orbital images of Mars that are of sufficient resolution to record wind ripple patterns on the surfaces of sand dunes. Ripple patterns provide valuable insights into aeolian erosion and deposition on Earth and Mars. In this study, we develop a systematic mapping procedure to examine sand ripple orientations and create surface process maps to evaluate the recent wind flow over the dunes, as well as the interplay of wind and dune shape. By carefully examining the morphology of the dunes and the location of grainflow and grainfall on dune slipfaces, the recent near-surface wind direction (short-term wind) can be identified. Results from the analysis of three dune fields on the floors of craters west of Hellas Basin show regional N, NW, SE, and ESE wind directions. In the three adjacent dune fields, surface process and flow maps suggest a complex wind pattern. The comparison of short-term wind with dune-constructing wind (long-term wind) shows NE and ESE winds may be persistent at least for the past thousands of years. The results also show that the orientation of inferred wind direction on linear dunes is correlated with the crestlines, which suggest that form–flow interaction may take place. The results of local wind flow documentation should improve Martian surface wind modeling and advance our understanding of sand transport, as well as the rates of sand mobility on both Mars and Earth.

1. Introduction

Mars has long been recognized as a planet where aeolian processes dominate the recent surface history (e.g., Greeley et al., 1992). Aeolian features, such as sand dunes and wind ripples, have been considered to be indicators of the surface wind regime (e.g., Greeley and Iversen, 1985). Many Martian sand dunes appear to be oriented transverse to the dominant wind (e.g., Zimbelman, 2003), so that dune and slipface orientations have proved useful to interpret the surface wind regime in several studies of sand dunes on Mars (e.g. Fenton and Richardson, 2001; Fenton et al., 2003; Ewing et al., 2010; Hayward et al., 2014). Distinct from sand dunes, wind-produced ripples are the smallest members of aeolian landforms (Bagnold, 1941). Wilson (1972) documented three scales for aeolian landforms; ripples (wavelength ~ 0.01–10 m), dunes (wavelength ~ 10–500 m), and draas (wavelength ~ 0.7–5.5 km), with the boundary between these categories not firmly fixed. Sharp (1963) pointed out that a ripple does not grow to become a dune, nor do dunes revert into ripples. Although the conclusions of Bagnold (1941) and Wilson (1972) are based on observations of dune fields on Earth, these basic descriptions should also be applicable to Martian aeolian features.

Ripples have been shown to be good indicators of local recent wind flow near the surface, a technique that has proved useful for evaluating the modification of sand dunes on Earth (Nielson and Kocurek, 1987) and Mars (Ewing et al., 2010). Ripple orientation was shown as a better indicator of wind flow over a dune than were the positions of sharp crests (Nielson and Kocurek, 1987). That is, the ripple patterns were used to identify the wind flow that caused modification of the dune crests, which were maintained as sharp features by multiple wind directions resulting from seasonal trends. Most previous studies of sand dunes on Mars did not utilize sand ripples to interpret the recent wind flow since the small-scale ripples were not observed except by rovers (e.g. Greeley et al., 2004; Sullivan et al., 2008) until the availability of very detailed orbital images obtained by the High Resolution Imaging Science Experiment (HiRISE) since late 2006 (McEwen et al., 2007, 2010).

* Corresponding author at: School of Earth and Space Exploration, Arizona State University, ISTB4-745, Tempe, AZ 85287, USA.
E-mail addresses: zacycliu@asu.edu (Z.Y.-C. Liu), zimbelmanj@si.edu (J.R. Zimbelman).

http://dx.doi.org/10.1016/j.icarus.2015.08.022
0019-1035/

HiRISE has provided the capability to obtain orbital images of Mars with a resolution of 25 cm/pixel (McEwen et al., 2007, 2010), which has provided important new insights into aeolian erosion and deposition on Mars (Bridges et al., 2007, 2010, 2011, 2012a,b, 2013; Bourke et al., 2010; Zimbelman, 2010; Gardin et al., 2012; Golombek et al., 2010; Hansen et al., 2011), including recent confirmation that movement of both ripples and dunes now can be documented from orbit (Silvestro et al., 2010; Chojnacki et al., 2011; Bridges et al., 2012a,b, 2013). HiRISE has imaged dark (low albedo) sand accumulations that typically show that ripples are evident on both dunes and sand patches (Fig. 1). The presence of sand ripples is an indication that local winds exceed the saltation threshold sufficiently often to either maintain or regenerate the ripple forms under conditions typical of the current thin Martian atmosphere, a situation that was generally not expected before the HiRISE data demonstrated that sand movement under present conditions occurs globally (Bridges et al., 2012a, 2013).

Dune wavelength should scale with the density ratio ρ_p/ρ_f between the particles and the fluid, for a given grain diameter (e.g., Durán et al., 2011; Hersen et al., 2002; Claudin and Andreotti, 2006). It has been shown that the wavelength at which dunes form scales with density ratio (Hersen et al., 2002; Claudin and Andreotti, 2006)—with a larger density ratio, dune wavelength generally appears to be larger. The Martian atmosphere is thin in comparison to that of Earth, with low pressure (mean surface air pressure: 6 mbar) and associated low density (~0.02 kg/m^3 at surface). Thus, the density ratio ρ_p/ρ_f on Mars is much larger than that of Earth. Moreover, wind stress derived from a given wind speed on Mars is lower than that at an equivalent speed on Earth, so sand is rather difficult to move on Mars. Once sand does move, however, the relevant length scales of the sand motion are rather long compared to Earth (e.g., White, 1979; Kok et al., 2012), so that both ripples and nascent sand dunes on Mars are typically much larger than their terrestrial counterparts. The low pressure of the Martian atmosphere causes it to respond quickly to surface temperature variations, and rapid changes in the temperature of the surface should drive strong wind (Fenton and Richardson, 2001). Although the 'fluid threshold' friction speed (i.e., the wind speed at which saltation is initiated) is much greater on Mars as compared to Earth (see Kok et al., 2012), saltation can be maintained on Mars by 'impact threshold' wind speeds an order of magnitude less than those required to initiate it (Kok, 2010). Typically the wind speeds are below the 'impact threshold' friction speed for Mars.

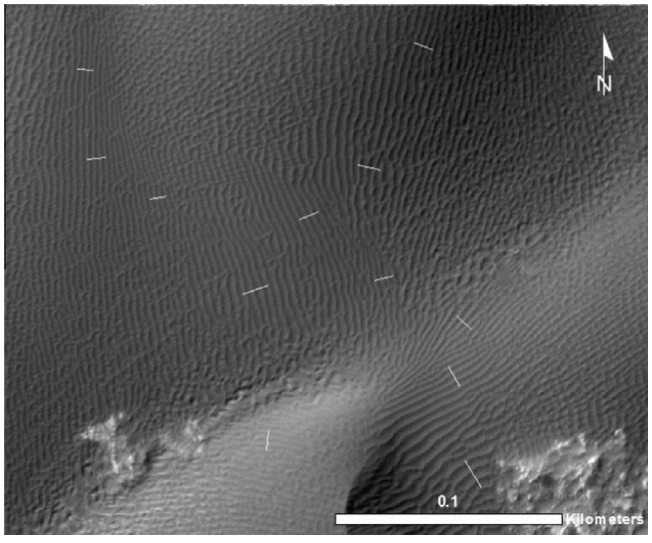

Fig. 1. Sand ripples on a HiRISE image, showing the mapping method for sand ripples used by Johnson and Zimbelman (2014; their Fig. 2). Mapped white lines represent the length across three ripple crests, oriented perpendicular to the ripples. Line azimuths include a 180° polarity ambiguity for the formative wind direction, unless other clues reveal the direction of wind flow. HiRISE images with a resolution of 25 cm/pixel that include dark (low albedo) sand accumulations typically show ripples.

Rubin and Hunter (1987) and Rubin and Ikeda (1990) introduced the concept of maximum gross bedform-normal transport (MGBNT), which states that the orientation of different types of dunes, such as transverse, oblique, and longitudinal, is determined by the wind regime. Thus, the dune types and orientations that emerge from specific wind regimes should be predictable. Fenton et al. (2014) developed a method to apply the rule of MGBNT and its inverse (IMGBNT) to predict the 'dune-constructing' wind regime (i.e., primary flow or long-term wind) based on an analysis of dune crestlines. The derived wind regime represents the long-term set of sand-transporting winds responsible for constructing dune fields, simplified versions of which have been used to facilitate modeling of the atmosphere, such as General Circulation Models (GCMs) (e.g., Pollack et al., 1990; Greeley et al., 1993; Anderson et al., 1999; Fenton and Richardson, 2001; Hayward et al., 2007, 2009, 2014).

GCMs indicate that the intensity and direction of global winds change throughout the course of a year. GCMs have produced simulations of various atmospheric and climatic conditions on Mars (e.g., Fenton and Richardson, 2001; Haberle et al., 2003). Gardin et al. (2012) examined the morphology of 550 dune fields in detail and they found that most are consistent with the GCM results, but some are not; this result may be due to local topographic forcing that is unresolved in current GCM models. They estimated that the turnover time of dunes (i.e., the time scale on which dunes should adapt to a new wind regime) is in the range of 10,000–100,000 Earth years, which is the same timescale on which obliquity changes may cause climate variations (Forget et al., 2006). However, Bridges et al. (2012b) found dune turnover time in Nili Patera is from 170 to a few thousand Earth years, suggesting that rapid migration rates/turnover times are expected, at least in some areas of Mars. In sum, sand dunes may provide a window into paleoclimate information, if the time scale can be constrained.

On the other end of the temporal spectrum, the more 'recent' near-surface wind regime (i.e., secondary flow or short-term wind) derived from ripple orientation potentially provides snapshots of local wind flow relevant to very recent or even current seasonal patterns. Such information (i.e., the short-term wind regime) would facilitate our understanding of current climate and atmospheric variations. Therefore, the recent near-surface wind information derived from present ripple orientations can provide constraints for atmospheric modeling at a new temporal and spatial scale, which is the main goal of this study.

Here we develop a technique to systematically map wind ripples on sand dunes using HiRISE images, and create surface process and recent wind flow maps to illustrate how ripple orientations are connected across a single dune. This study was conducted in order to expand upon the recent findings of Johnson and Zimbelman (2013, 2014, 2015) (Fig. 1) who mapped ripples on small dunes globally on Mars and inferred local wind directions. Rather than investigating small dunes globally, this study focuses on producing detailed interpretative maps for one region on Mars. In addition, the resulting maps carefully documented ripple orientations, dune morphology, distribution of frost, grainflow and grainfall on slip faces, not only to evaluate the local wind patterns (Fig. 1) but also the most recent wind directions. The results of local wind flow patterns are anticipated to improve local-scale wind modeling as well as more regional-scale atmospheric circulation modeling, all of which should facilitate comparison with published data from terrestrial sand dune fields. Moreover, this study also aims to explore the question for aeolian processes of the degree to which wind may alter dune shape, or vice versa (i.e., the interplay of wind and dune

shape, or form–flow interaction) (Hugenholtz and Wolfe, 2009; Walker and Nickling, 2002). The results of this study should provide insight into this question.

This report first describes the region on Mars where individual dunes were mapped using released HiRISE images. Next the ripple mapping procedure is described, from which the results of interpreted local wind flow and surface process maps were derived. Finally, broader implications of ripple pattern mapping and associated wind regimes are discussed.

2. Study regions and HiRISE dataset

The study regions are located west of Hellas Basin in the southern hemisphere of Mars. Fig. 2 shows the locations of the three mapped dune fields, along with five HiRISE image footprints. Linear dunes are common in sand deposits within large impact craters in the southern highlands of Mars (Hayward et al., 2007, 2014). The ripple patterns within linear (also known as longitudinal) dunes are more straightforward and easier to map compared with those of star dunes and other complex dunes. Thus, we chose to map linear dunes while initially developing the mapping technique (Map #1). Other types of dunes were chosen for analysis following the mapping technique established for linear dunes (Maps #2–5). We chose five HiRISE images for this study, which contain complete and well-developed dune fields within large impact craters, including the Proctor crater dune field. Maps #2–4 are dedicated to the same dune field in Proctor crater studied by Fenton et al. (2003). Fenton et al. (2003) studied the dunes in Proctor crater, a 150 km diameter crater in Noachis Terra, and they interpreted the dune-constructing wind regimes (long-term wind) based on the dune slip faces, which are compared with the recent near-surface wind regime (short-term wind) interpreted by ripple patterns in this study (see Section 5.3). Table 1 summarizes the details of the five HiRISE images, including the coordinates of the center of the image, spatial resolution, solar longitude, season at the time the image was taken, and dune type. The five mapped dune fields contain different dune types: linear, star, and barchan dunes. A HiRISE stereo pair and a publicly released Digital Terrain Model (DTM) are available for Map #3 (HiRISE DTM: DTEEC_003800_1325_004077_1325_U01; resolution ~ 99 cm/pixel).

3. Methodology

3.1. Mapping procedure

We adapted the mapping method used for dunes on Earth by Nielson and Kocurek (1987) who mapped sedimentary processes and inferred surface airflow. We established a procedure to (1) map sand ripples on Mars in HiRISE images, and (2) interpret the direction of local wind and airflow. We first define the mapping units, which include primary crestlines, secondary crestlines, ripple crests, transverse aeolian ridges (TARs), frost, grainflow/grainfall, wind direction and inferred airflow (Figs. 3a and 4). Secondary crestlines are generally shorter and are mapped based on their orientation >60° apart from the general trend of primary crestlines. To distinguish ripples from TARs, TARs typically have wavelengths of 20–60 m and are as bright or brighter than the surrounding terrain (Wilson and Zimbelman, 2004), while ripples have wavelengths < 5 m and are typically found on dark (sand) deposits. We incorporated the HiRISE images into ArcGIS and created shapefiles for lines and polygons with different colors. Lines were drawn to trace the ripple crests and dune crestlines. Polygons were drawn to define the boundaries of frost, as well as grainflow and grainfall on dune slip faces. Color codes used for the mapping units are shown in Fig. 4. In addition, we standardized the ripple symbol to capture pattern variations without substantial oversampling; here each ripple symbol is mapped with a spacing of 60–100 m and with a length of 60–100 m on the map. We also standardized an indicator to assess the density of ripple crests (DR), where DR = total length (m)/dune area (m^2). By evaluating the ripple distribution according to the resolution of HiRISE images, we determined that the DR ~ 5–7 (100 m^{-1}) is appropriate to avoid oversampling and clutter in the maps. We followed a similar sampling standard used for sand ripples to map TARs. After completing the mapping of crestlines, ripple crests, frosts, grainflow/grainfall, and TARs, we then inferred the airflow and wind direction according to the ripple crests. Airflow is shown by a long arrow with an arcuate shape, and wind direction is indicated by a short arrow. Both attributes are interpreted and mapped perpendicular to ripple crests. In other words, wind direction and airflow are derived from the analysis of both ripple crest orientation and dune shape. The arc-shaped airflow path is also mapped following the morphology of the dunes (i.e., the curving shape of the dunes). See Fig. 4 for an illustration of the mapping units on a HiRISE image. Using the mapped units of dune crests, ripples, and wind directions, the final surface process and airflow map was completed (following Nielson and Kocurek, 1987). In this study, since TARs are often off the dune surface in our mapping regions, TARs are neither used to infer the local wind direction nor to the related wind flow analysis.

The mapped line orientations give the azimuth of the aeolian bedform (following Johnson and Zimbelman, 2014). In our mapping of each HiRISE image, the mapped shapefile units that were lines included primary crestlines, secondary crestlines, ripple crests, TARs, and wind directions. We extracted the azimuths from the shapefiles of crestlines, ripple crests and wind directions to create rose diagrams, which are length-weighted by division into segments of constant orientation. Rose diagrams highlight the dominant orientation of crestlines, ripple crests and wind directions. Note that the rose diagrams of wind direction here are from the derived vectors (see Section 4). By analyzing the rose diagrams of each map unit, we can evaluate whether there is a correlation between the orientations of dune crests, near-surface wind regimes, and ripple patterns.

3.1.1. Differentiation of ripple patterns

In HiRISE images, the wind ripples are visible on dark dunes and the ripple orientations near the dune brink can be identified with confidence (Fig. 3). However, there may be more than one visible ripple pattern on a single dune, which may have been formed at different times by more than one different wind orientation (Fig. 3b); thus, it is difficult to determine the overall flow by considering all ripples at once. In this study, we first separate out different ripple patterns and then figure out the wind that formed each pattern, rather than mapping out wind directions all at once. Fig. 3b shows an example of differentiating two ripple patterns along a dune brink. Ripple pattern 1 has a NW/SE trend and pattern 2 has a NE/SW trend. They are formed from two different wind flows because there are places where the pattern overlaps (where two dash-lines cross). Two overlapping ripple patterns imply that either one pattern is partially overwritten by another, or the area routinely experiences winds from two different directions and the ripples have grown in response to both winds. For the five mapping areas in this study, we separate out two ripple patterns and interpret the winds according to these ripple trends. It is possible that there may be more than two ripple patterns in the star dune areas, but for simplicity, in this study we only differentiate two main wind ripple patterns (ripple pattern 1 and ripple pattern 2) and the corresponding two wind directions (wind direction 1 and wind direction 2) (see color codes in Fig. 4). Ripple pattern 1 is generally more abundant than ripple pattern 2, but there is no

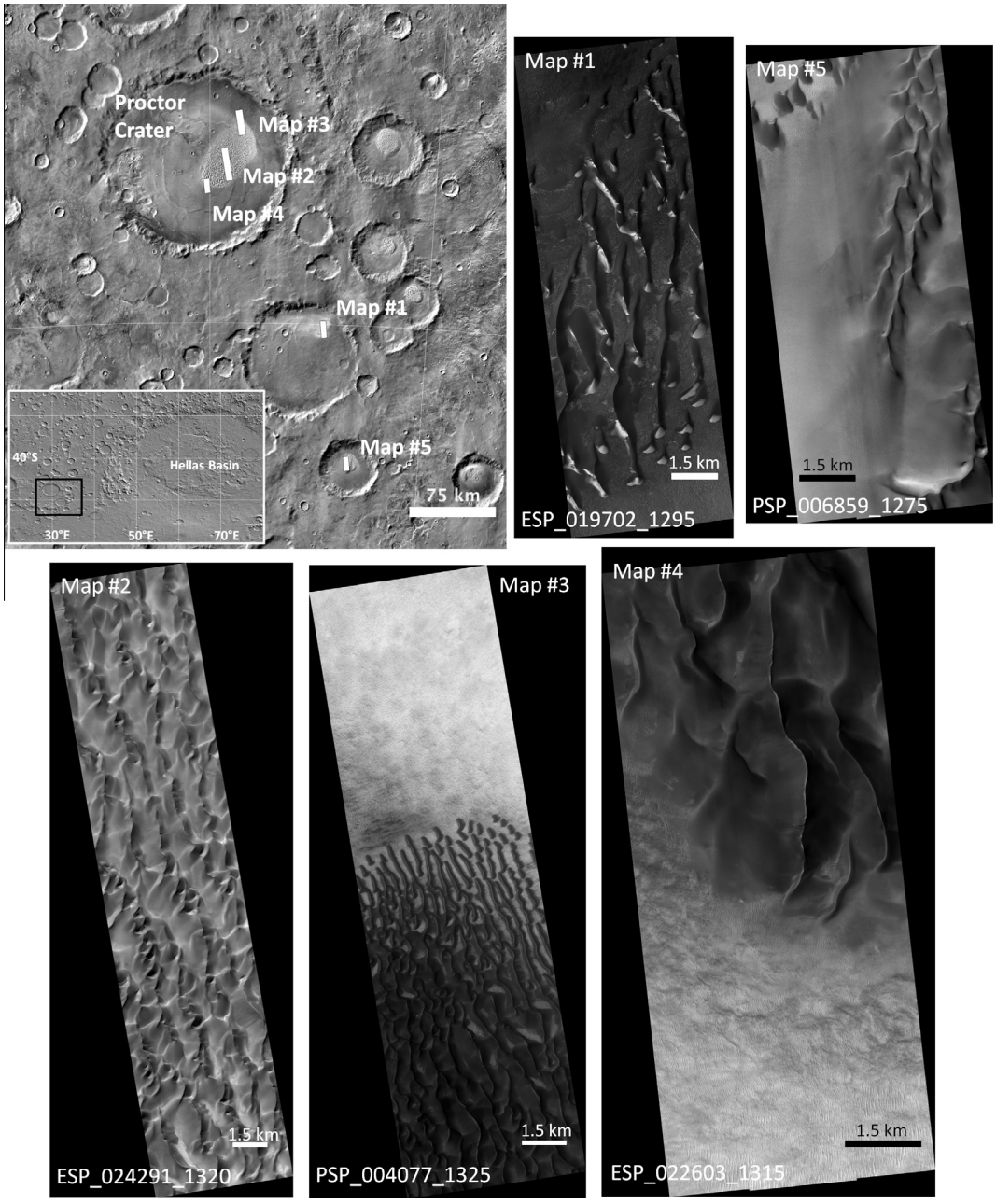

Fig. 2. Locations of the three mapped dune fields, along with the corresponding HiRISE browse images. Maps #2–4 are for portions of one large dune field in Proctor crater. Left top image shows the locations of the three studied dune fields, as well as the five HiRISE stamps (in white). The background image is from the THEMIS day-time mosaic database (Christensen et al., 2003). The white-outlined inset shows the regional setting, including the Hellas Basin. Black box in the inset shows the location of left top image. Details for the five HiRISE images are summarized in Table 1.

Table 1
Summary of HiRISE images for Maps #1–5.

Map #	HiRISE	Description	Longitude (°)	Latitude (°)	Resolution (cm/pixel)	Ls (°)	Season	Dune type
1	ESP_019702_1295	USGS dune database	32.62	−50.7	50	161.4	Winter	Linear
2	ESP_024291_1320	Proctor crater dune changes	30.37	−47.65	58.3	9.2	Autumn	Linear/Star
3	PSP_004077_1325	Proctor crater dune field	30.67	−47.04	28.2	254.6	Spring	Linear/Star
4	ESP_022603_1315	Proctor crater dune margin changes	29.94	−47.98	25.5	298	Summer	Star
5	PSP_006859_1275	High thermal inertia central material in crater	33.27	−52.06	25.4	16.7	Autumn	Barchan/ Crescentic
DTM	DTEEC_003800_1325_004077_1325_U01	Proctor crater dune field	30.67	−47.04	99	240.9 254.6	Spring	Linear/Star

Dune type from MGD[3] (Hayward et al., 2007).

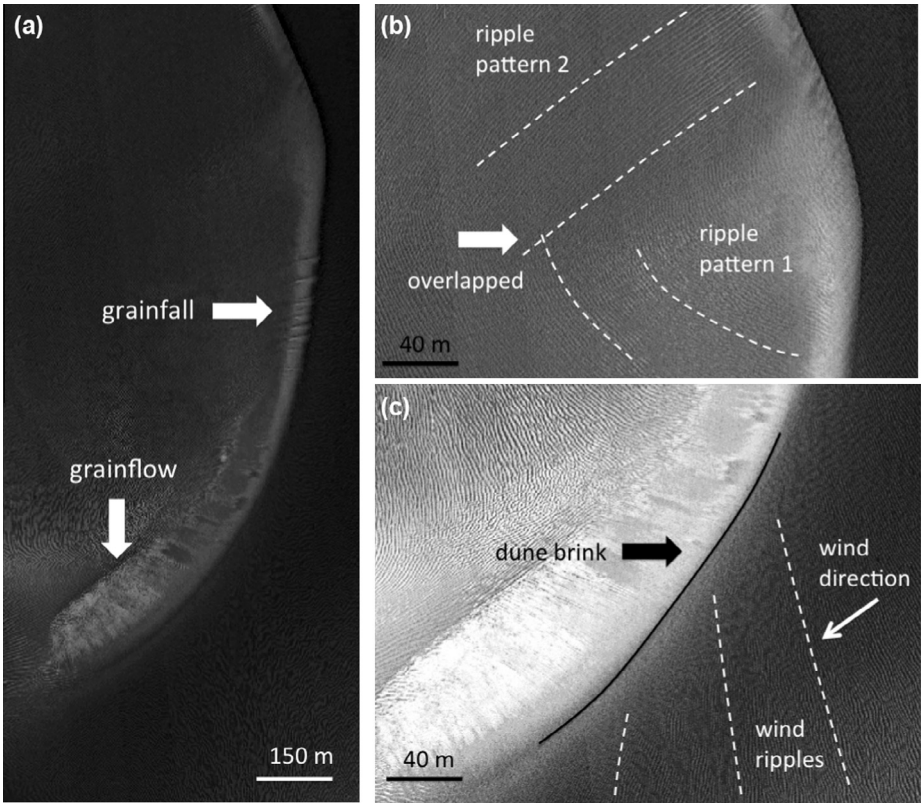

Fig. 3. (a) Example of grainflow and grainfall deposits (indicated by white arrows) in the lee of slipfaces on sand dunes (in Map #4). (b) Two wind ripple trends are identified on the western side of a dune. Ripple pattern 1 has a NW/SE trend and pattern 2 has a NE/SW trend. White arrow indicates where two ripple patterns overlap. (c) The NW/SE ripples suggest that they were formed by a wind ranging from NE to SW, because the ripple pattern extends up to intersect obliquely with the dune brink on the eastern side of the dune. Note that all three images include adjusted contrast and image sharpness to better show the wind ripple patterns.

implication here for the relative timing during which either pattern formed.

3.2. Indicators to resolve wind directional ambiguity

Johnson and Zimbelman (2013, 2014, 2015) have mapped ripples in dune fields globally distributed around Mars, and have interpreted a wind pattern with an uncertain polarity (±180°) instead of the actual orientation. In this study, we use overall dune shape, dune brink, ripple morphology, and the location of grainflow and grainfall to facilitate the interpretation of the most recent wind directions in the studied dune fields.

3.2.1. Ripple morphology

Aeolian ripples are indicative of a flow configuration where impact splash dominates. Examining the sand ripple morphology along a dune brink may reveal the actual wind flow direction. Fig. 3c (in Map #4 region) shows the NW/SE ripples were formed by a wind ranging from NE to SW, because the ripple pattern extends upslope to intersect obliquely with the dune brink on the eastern side of the dune. Ripples can March obliquely up the windward side of a dune until they hit the brink, but it is unlikely that ripples formed due to the wind blowing from the side along the steeper slope. In Fig. 4, the ripple pattern 1 (in purple color) and the corresponding wind direction (in green color) are interpreted with ripple morphology along the dune brink.

3.2.2. Grainflow and grainfall

Grainfall generally occurs as saltating grains on the stoss slope fly over the brink and settle upon the lee face. Grainflow occurs as the upper lee face steepens from grainfall accumulation and then fails at the static angle of repose (avalanching) (Hunter, 1977). Although grainflow and grainfall are related to gravity-driven processes, they can be indicators for interpreting near-surface wind direction along the dunes. Few grainflow/grainfall areas are observed on the dunes in our five mapping regions (Fig. 4a). Nielson and Kocurek (1987) and Ewing et al. (2010) made surface process maps indicating airflow direction, whose interpretations are facilitated by the locations of grainflow (avalanching) and grainfall in the lee of slipfaces on the dune. Grainfall indicates that grains fall to the surface in the area of reduced wind speeds (Nielson and Kocurek, 1987). Nielson and Kocurek (1987) suggested that localized grainflow occurs as fluctuations in wind direction and grainflow can be triggered by the wind locally exceeding the threshold. Thus, on the downwind side of dunes, grainflow deposits occur in regions of relatively strong winds that destabilize the upper lee slopes, whereas grainfall occurs where wind speed is reduced, allowing grains to become decoupled from the wind flow and fall out on to the surface. Examples in Fig. 4a and b (Map #4) show that the wind (blue arrows) would be expected to blow from SE across dune crestline in order to produce grainflow deposits on the downwind side of the dunes; another direction of wind (green arrows) would be expected to blow from NE to form the grainfall deposits in the reduced wind speed regions downwind of a crest. The wind direction interpreted from the grainfall is consistent with that from ripple morphology along the dune brink (see Section 3.2.1) in the same region. Fig. 4c shows that if the wind blows from the opposite direction, the grainflow would be expected to occur on the indicated area (the dashed polygon) along the eastern slopes of the dune by a

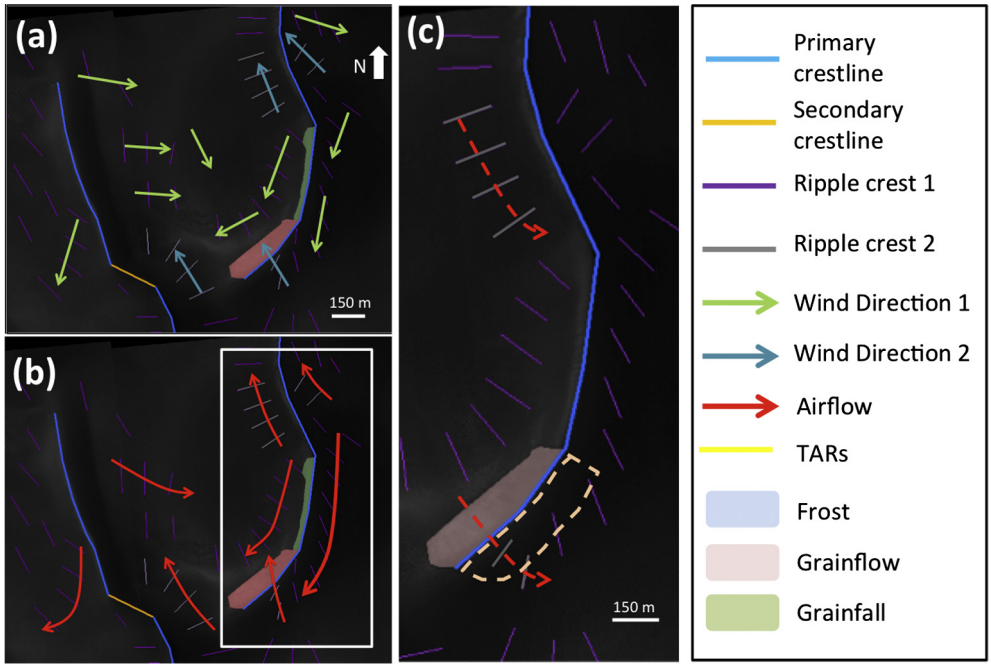

Fig. 4. (a and b) Example of a surface process and airflow map. Symbol legends are shown in the right column. Symbol legends are uniform in Figs. 4–6. There are 11 mapped units: primary crestline (blue), secondary crestline (orange), ripple crest 1 (purple), ripple crest 2 (gray), TAR (yellow), near-surface wind direction 1 (green), wind direction 2 (cadet blue), near-surface airflow (red), frost (light blue), grainflow (light pink), and grainfall (light green). The mapped purple and gray lines are aligned with dune ripple crests by careful examination of the HiRISE image along with the density of ripples (DR) indicator, to avoid over-sampling (see Section 3.1). The inferred airflow patterns are generally correlated with the orientation of the crestlines. Actual wind direction interpretation is based on the location of grainflow and grainfall deposits and ripple morphology along dune brink (see Section 3.2.2). The grainflow area is on the lee side of the dune. In order to produce the grainflows on the NW dune slope, wind was blowing across the crestline probably from SE. The white rectangle indicates the location of part (c). (c) The expected grainflow location (dashed pink polygon) if the near-surface wind had been blowing from NW instead of SE.

NW wind. This has not happened, so it is likely that the ripple crest 2 pattern was formed by the same SE wind that produced the observed grainflows.

3.2.3. Dunes near the southern pole

Polar temperatures during winter in both hemispheres get low enough to condense carbon dioxide and water to form seasonal polar caps on Mars. The deposition of CO_2 frost (high albedo) on polar dunes is evident when the dunes are observed from orbit during winter or spring (e.g., Kieffer et al., 2006; Hansen et al., 2011; Piqueux and Christensen, 2008). Avalanches of dark sand are occasionally visible over some of the bright frost (e.g., Fenton et al., 2003; Edgett and Malin, 2000). When CO_2 gas builds up under the frost cover in spring and escapes suddenly through cracks in the frost where sand and dust are ejected, the ephemeral dark spidery patterns are formed (Hansen et al., 2010). Thus, frost streaks may potentially reveal additional wind orientation information (French and Gierasch, 1979; Howard, 1980; Thomas et al., 1979; Thomas, 1981). Based on the analysis of frost streaks, Thomas et al. (1979) suggested a prograde circulation pattern of near-surface winds around the southern pole (55–90°S) with a definite component away from the pole. They found evidence that showed this wind pattern persisted throughout the winter. Therefore, this wind pattern can be adopted for the dune fields around the southern pole in wintertime. Our five chosen mapping regions (Maps #1–5) are located in southern mid-latitudes (47–52°S); only HiRISE image of Map #1 was taken in the southern winter. Thus, with the assumption of wind blowing away from the pole (i.e., SW wind direction) during winter, examples of dunes in Map #1 (Fig. 6a) show that the wind would be expected to blow from the south. In addition, the global wind pattern predicted by Fenton and Richardson (2001) show a consistent wind direction (wind blows away from the pole) for the Map #1 region of west Hellas Basin during southern winter. Note that this S–N wind regime is only applicable to the dunes around the south pole in wintertime. During spring and fall, CO_2 ice patches are expected only to remain on pole-facing slopes of mid-latitude dunes. This suggests that the location of frost patches is mainly controlled by the reduced insolation on shaded slopes of mid-latitude dunes during spring and fall.

In summary, the wind directional ambiguity is resolved by incorporating the analysis of ripple morphology along the dune brink and the distribution of grainflow and grainfall locations, along with previous studies in the region. We applied the procedure described in this section to the mapping regions in the five HiRISE images. There are other options to facilitate determining the ripple-forming wind direction, such as wind scours (Bishop, 2011) and investigation of overlapping HiRISE images from different seasons. However, no wind scours were found in our images, and no overlapping HiRISE images from different seasons are available in our mapping regions; we suggest that these options should be considered in future work.

3.3. Incorporation of digital terrain model

A publicly released HiRISE DTM (DTEEC_003800_1325_004077_1325_U01; Fig. 5) is available for the study area that includes Map #3, which was useful to analyze and evaluate the effect of surface slope. It has been shown that on a sloping sand surface, the downwind direction interpreted to be perpendicular to the ripple crests is actually deflected down-gradient as a function of the local surface slope on the dune; Howard (1977) gives a mathematical expression for how surface slopes on a sand dune can affect the orientation of ripples with respect to the formative winds. Thus, we

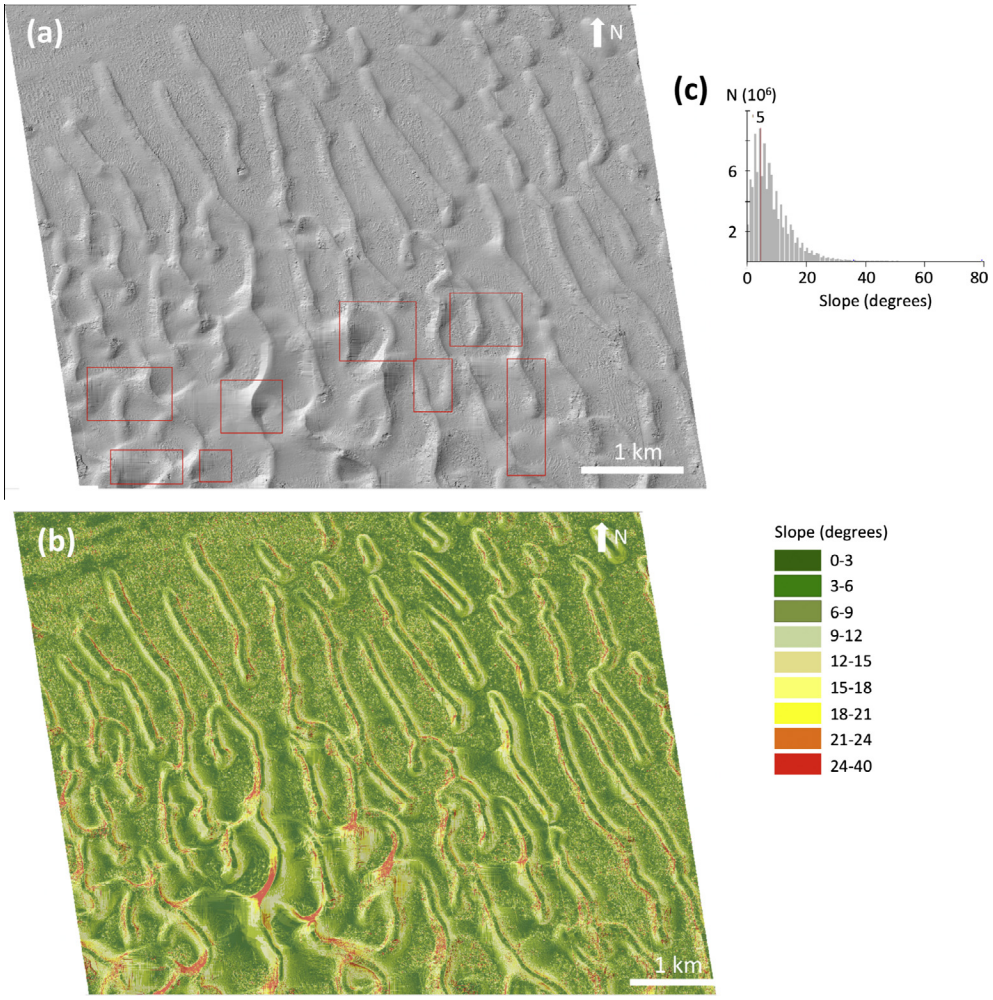

Fig. 5. HiRISE digital terrain model (DTM) DTEEC_003800_1325_004077_1325_U01 corresponding to a portion of Map #3. (a) DTM hillshade image clearly shows the morphology of both linear (upper right) and star (lower center) dunes. The sunlight for the shading comes from the left. The red rectangles indicate the areas with numerous artifacts. (b) Slope map generated from the HiRISE DTM. Green to tan colors cover the slope angle < 15°, where ripple deflection angles should be <27° with respect to the actual surface wind direction, based on Howard (1977). (c) Histogram of slopes sorting by slope angle at each pixel point (N) show that overall slopes are predominantly <20°, with few slopes greater than this. Howard (1977) shows that the deflection angle becomes more significant when slope >20°, such as near a slip face. Most of the mapping area and interpreted wind directions are within green to yellow regions. Thus, slope effects are expected to play a minor role in wind direction interpretations.

used the DTM data to evaluate the dune surface slope effects on the interpreted near-surface wind regime for the study region covered by Map #3 (see Section 5.1).

4. Results

Completed surface process and airflow maps (Maps #1–5) are shown in Fig. 6a–e, following the mapping procedure described in Section 3. The corresponding wind rose diagrams are also presented in Fig. 6, along with rose diagrams of primary crestlines, secondary crestlines, and ripple crests. Ripple patterns provide valuable information about recent wind flow and the identification of localized wind patterns. Each wind rose is a polar diagram, where the wind direction is binned into 8, 12, or 16 azimuth sections, and the length of the radiating bar or wedge at each azimuth corresponds to the relative frequency with which the described attribute aligns with that direction. Wind rose diagrams show dominant near-surface wind directions for each dune field. The colored arrows on rose diagrams (Fig. 6) indicate the mean directions for primary crestlines, secondary crestlines, ripple crests, and dominant wind directions for each dune field. Fig. 7 shows the locations of the five mapped HiRISE image stamps and the recent near-surface wind directions inferred by each wind rose. The dominant wind directions in the five study regions show general N, NW, SE, and ESE orientations. Note that the interpreted wind directions of Map #2–4 blow from N to S, whereas Map #1 and #5 show wind from S to N. The results of the dominant orientation of winds and crestlines are summarized in Table 2.

A publicly released HiRISE DTM (Fig. 5a) was used to generate a slope map for the Map #3 area (Fig. 5b). The HiRISE image stereo pairs (PSP_003800_1325 and PSP_004077_1325) used to generate the DTM were obtained 22 Earth days apart, which aided the DTM generation since it is often difficult for automated feature matching software to work well on sand dunes if the ripples may have moved during the time between when the images were obtained. Consequently, any details about sand ripple change are missing from the DTM, plus there are many artifacts on the sand dunes themselves and in the interdune areas. However, the DTM was still useful for providing first-order slope information about the dunes within Map #3 (see Section 5.1).

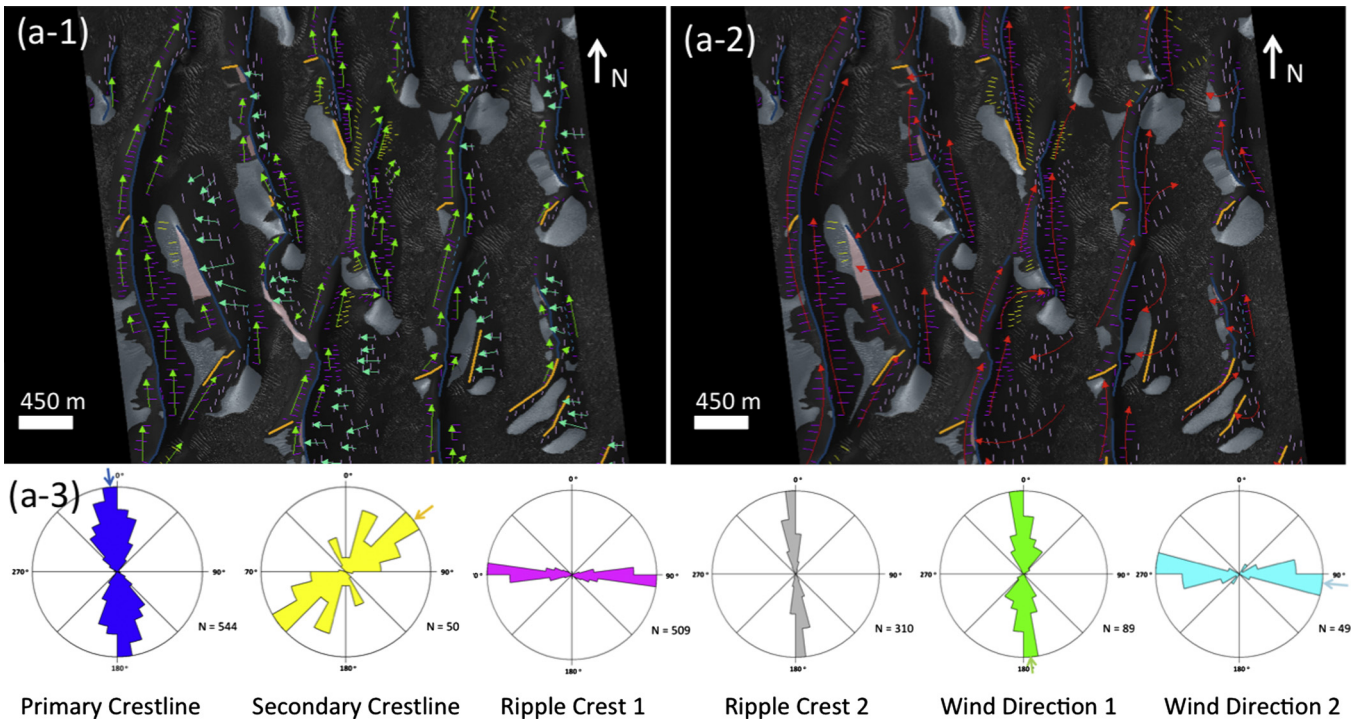

Fig. 6a. Final surface process and airflow maps (for Map #1) for linear dunes. Color codes for map units can be found in Fig. 3. (a-1) Interpreted near-surface wind directions are S and E. The season when the image was taken is winter, so frost deposits are present on some dunes. (a-2) Arc-shape airflow directions (S–N). The map shows that airflow patterns are correlated with dune crest orientation. (a-3) Rose diagrams of mapped crestlines, ripple crests and interpreted wind directions. Wind direction (green) has a clear correlation with the orientation of primary crestline (blue), which implies possible form–flow (see Section 5.2). The small colored arrows on the rose diagrams indicate the dominant directions of primary crestline, secondary crestline, ripple crest, and inferred near-surface wind directions.

Table 2
Summary of wind directions derived from wind roses for Maps #1–5.

Map #	Wind blow direction 1 (azimuth)	Wind blow direction 2 (azimuth)	Season
1	S (355°)	E (275°)	Winter
2	N (170°) N (184°)	ESE (292°)	Autumn
3	N (175°) NW (137°)	ESE (294°)	Spring
4	NE (224°) N (185°) NNW (158°)	SE (314°)	Summer
5	SE (314°)	N (180°) E (260°)	Autumn

5. Discussion

5.1. Near-surface wind regime and slope effect

The shape of the sand dunes and the location of grainfall, and grainflow deposits indicate the local wind flow direction at the three studied dune fields. Surface process maps for three adjacent dune fields show variations in the local wind regime (Fig. 7) – the interpreted near-surface wind direction for Map #1 and Map #5 is from S to N, while the wind directions of Maps #2–4 are generally from N to S. This suggests that surface wind patterns are complex in the study area. Since all three-studied dune fields are within large craters, the topography of the craters may play a role in shaping local winds, for example, due to differential heating within the crater interior. Generally, solar-heated slopes will experience upslope flow as the warm air rises, and cooler slopes will experience downhill flow (e.g., Greeley et al., 2003; Hayward et al., 2014). Thus, the near-surface wind regime within craters may change diurnally and seasonally. It is noteworthy that differential heating is a factor to shape local winds, however, the topographic relief itself may be a greater contributor in shaping local winds. Mapping of dune fields within adjacent craters would be required to investigate a possible correlation between near-surface wind regime, dune location within the crater, and topography of the crater.

Parteli et al. (2009) used numerical models to show how the wind regime shaped the morphology of sand dunes, forming different types of dunes. They concluded that when winds are above the saltation threshold friction speed and thus strong enough to cause sand transport, and the wind blows predominantly from a single direction, then transverse dunes are likely to result. If sand-moving winds are bimodal, coming from opposite directions, then linear dunes are expected. If the directions between multiple winds are highly variable, coming from three or more directions, then star dunes will likely form. Other previous work also confirmed the formation of various types of dunes in varied directional wind flows (e.g., Rubin and Ikeda, 1990; Reffet et al., 2010). Based on the wind roses (Fig. 6e), barchans in Map #5 (northwest part of Map #5) have crestlines in two distinct orientations, indicating their modification by two separate winds. The influence of both winds is even more apparent in the nearby linear dunes (southeast part of Map #5). This is in good agreement with a model prediction by Parteli et al. (2009). Map #1 indicates a bimodal wind regime and the observed dune type is linear; Maps #2–4 show star dunes and the surface process maps suggest the presence of two or three prominent wind directions, again consistent with the model (e.g., Parteli et al., 2009; Fenton et al., 2003).

The slope effect discussed in Howard (1977) presents an equation to estimate the deflection of the formational wind direction:

$$\sin\beta = \frac{\tan\theta \sin\gamma}{\tan 30.5^\circ}$$

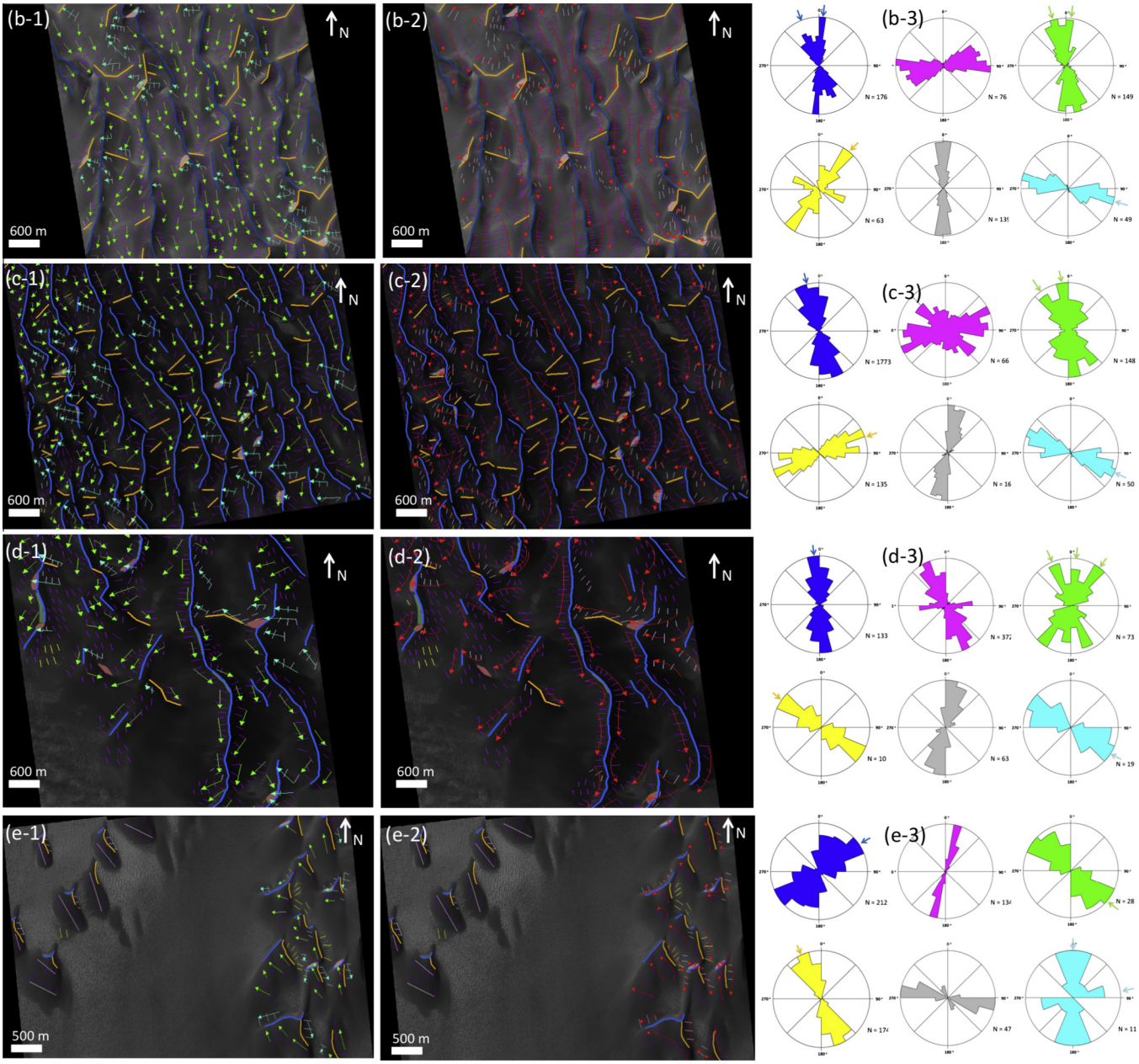

Fig. 6b–e. Left column has the surface process maps and inferred wind regime corresponding to Maps #2–5. Middle column has corresponding surface process maps with airflow. Right column has rose diagrams for crestlines, ripple crests and near-surface wind directions. The small colored arrows on the rose diagrams indicate the dominant directions of primary crestline, secondary crestline, and inferred wind directions. The dune field in (b) Map #2 is a combination of linear dunes and star dunes. Correlation of wind direction and primary crestline orientation is evident. (c) Map #3 shows mature star dunes. The wind roses show near-surface winds blow in more than three directions to form star dunes (Parteli et al., 2009). Correlation between wind regime and crestline is unclear. (d) Map #4 contains a combination of linear dunes and star dunes. The correlation of wind direction and crestline orientation is unclear. (e) Map #5 has barchan/crescentic (northwest) and longitudinal (southeast) dunes. The actual wind direction of the dunes in the northwest portion of the image cannot be interpreted due to the lack of grainfall/grainflow; white lines show a bimodal wind direction. Wind rose shows a 90° difference as compared to the primary crestline orientation, but wind direction 1 (green) is correlated with secondary dune crest.

where β is the observed ripple deflection, θ is the dune surface slope, and γ is the angle between the wind and the surface gradient. The slope map from the DTM data (Fig. 5b) shows that the slopes on the stoss sides of sand dunes in Map #3 are generally <15°. A histogram of slopes (Fig. 5c) shows that the overall slopes are generally <20°. Thus, the Howard equation indicates ripple deflection angles should be <27° with respect to the actual surface wind direction, which will not significantly change the inferred surface wind directions that are derived from the ripple orientations documented on the maps. However, areas of steep slopes (such as near slip faces) should be avoided for deriving wind orientations from ripple measurements.

5.2. Form–flow interaction

Rose diagrams of crestlines, ripples and wind directions (Fig. 6) indicate that the interpreted local wind direction is correlated with the dune crest orientation. The histograms of wind direction azimuth for the five maps (Fig. 8) show correlations between the orientation of crestlines and wind patterns to varying degrees. This

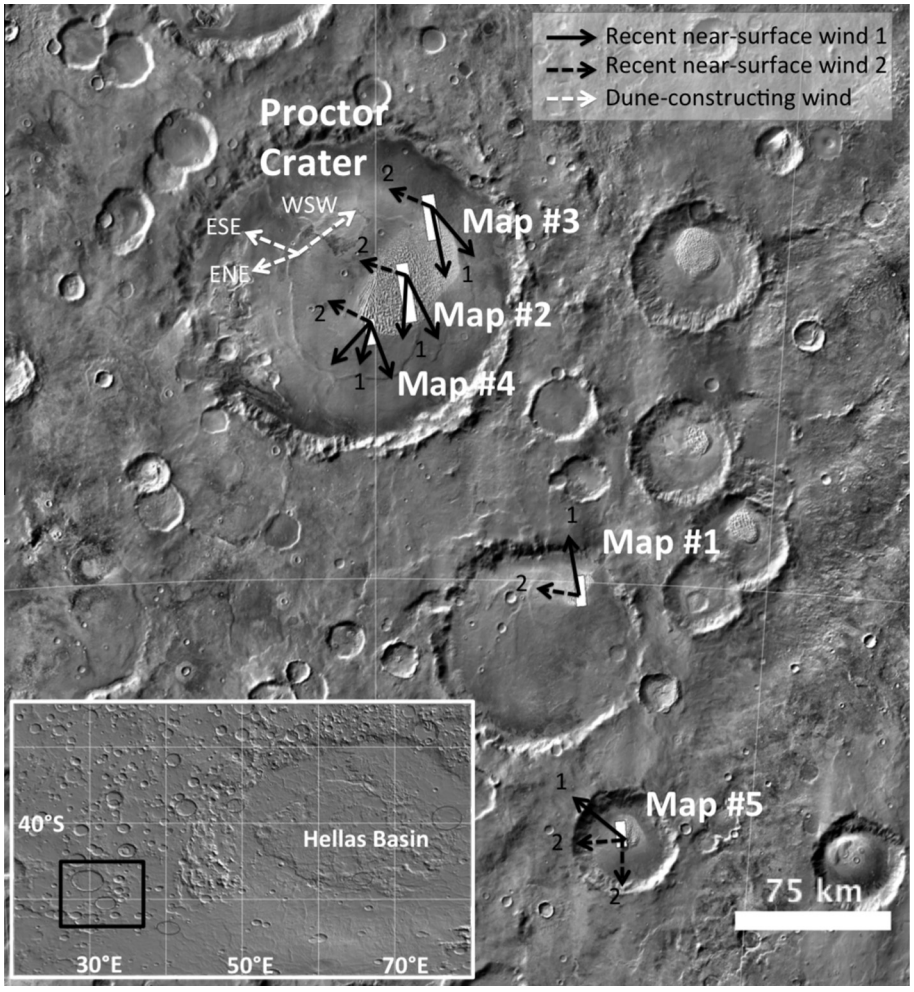

Fig. 7. The inferred near-surface wind regime for the three studied dune fields. Black arrows with numbers on HiRISE stamps indicate the wind directions inferred by the wind rose 1 (green) and wind rose 2 (gray) (Fig. 6). Details of inferred near-surface wind directions are summarized in Table 2. White dash arrows are the long-term dune-constructing wind directions. Fenton et al. (2003) suggested the WSW, ESE, and ENE direction winds have constructed the dunes within Proctor crater.

result suggests the possible presence of form–flow interaction (Hugenholtz and Wolfe, 2009; Walker and Nickling, 2002). Form–flow interaction have been recognized as an important control on dune shape, size, and spacing, but also dune size and spacing exert a significant influence on flow patterns, so that there is feedback between all of these factors (Walker and Nickling, 2002). Large bedforms, such as dunes, generate pressure gradients in the wind flow field, which cause flow streamlines to diverge from their primary direction (i.e., long-term dune-constructing wind) when passing around or over the dune bedform while the wind flow also continuously contributes to shape and construct the dunes; hence, there is a significant interplay between wind flow, dune shape, and crestline orientation.

The histograms of Fig. 8a suggest that the crestlines of linear dunes in Map #1 are correlated with the dominant wind direction. However, histograms of star dunes (Maps #2–4) do not show a clear correlation between crestline orientation and wind pattern (Fig. 8b–d), consistent with complex wind flow being responsible for the star dune shapes. In Fig. 6e, the wind rose for Map #5 shows the dominant wind direction that appears to be 90° from the primary dune crest orientation, but which is correlated with the secondary crestline orientation. Taken together, these observations suggest that dune shape and crestline orientation have altered the near-surface wind (i.e., the short-term wind), which indicate that form–flow interaction and dune shape both may exert control on wind flow patterns locally. However, the short-term wind that forms ripples is unrelated to dune construction. In addition, dune crestlines in our mapping regions appear crisp, suggesting that present-day winds (i.e., the long-term wind) may still contribute to dune construction. This means that the correlation between dune crestline and inferred wind direction shows that dune shape and crestline orientation both may have altered near-surface wind regimes, but it is not clear if short-term wind has recently contributed to shape the dune morphology. Acknowledging that form–flow interaction is a complex aeolian process, future work is needed to evaluate the presence and intensity of form–flow interaction, such as examination of future overlapping HiRISE images from different seasons to further document the ripple patterns and wind regimes in the mapped dune fields.

5.3. Long-term wind vs. short-term wind

The near-surface wind directions for the Procter dune field (Maps #2–4) are generally NE, and ESE. Fenton et al. (2003) examine dune slipfaces using Mars Orbiter Camera images to determine the 'dune-constructing' wind regimes (long-term wind) for the dunes in Procter crater; their results show that the dune-constructing wind generally blows along WSW, ENE, and ESE directions (Fig. 7). In light of form flow interaction likely taking place, we consider that the dune-constructing wind regimes inferred by

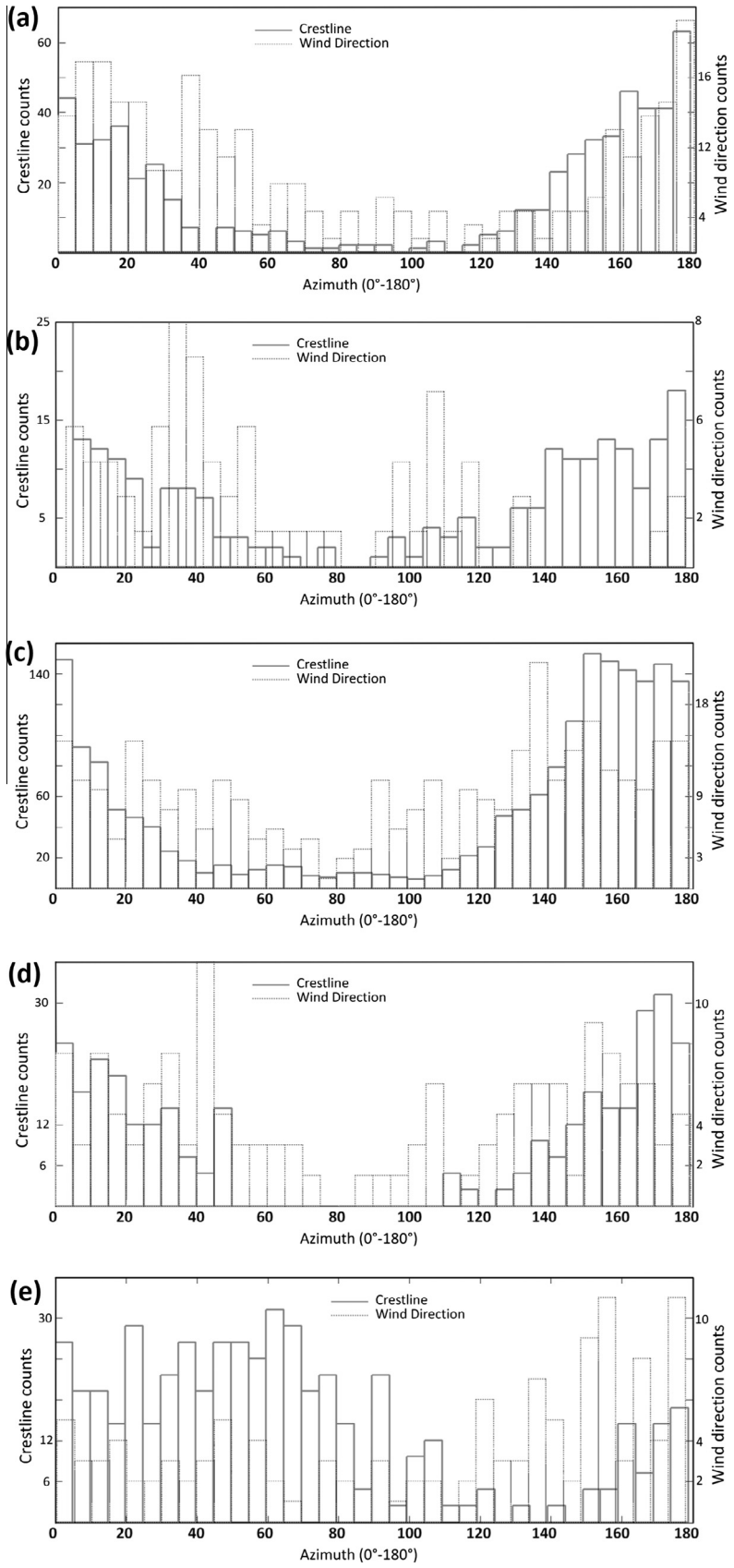

Fig. 8. Histograms of wind direction azimuth (0–180°) and dune crest orientation. (a) Wind rose of Fig. 5a and Map #1. (b)–(e) correspond to the wind roses of Fig. 6b (Map #2), Fig. 6c (Map #3), Fig. 6d (Map #4), and Fig. 6e (Map #5), respectively. The dashed line corresponds to histograms of wind direction azimuth and solid line corresponds to histograms of dune crest orientation, including primary and secondary crestlines. (a) The dune type in Map #1 is linear, and the histogram shows the correlation of wind flow and dune crest. (b–d) The dune fields of Maps #2–4 in Proctor crater are star dunes. More than three wind directions are shaping the star dunes in Map #2–4; a correlation between dune crestline and wind pattern is not evident. The dune type in Map #5 is barchan/longitudinal dunes. (e) Histogram shows that the inferred wind direction is about 90° away from the dune crest orientation.

slipface orientation (Fenton et al., 2003) are 'long-term' wind regimes that are initially responsible for forming the dunes, whereas the near-surface wind regimes inferred from sand ripples are more closely related to form–flow interaction, and thus may be only a 'snapshot' of the most recent wind pattern. Based on our analysis (Fig. 7), long-term wind regime is similar with short-term wind pattern, except for the long-term WSW wind. Thus, assuming an appropriate dune turnover time (Bridges et al., 2012b), the NE and ESE winds may be persistent at least through the past thousands of years.

The dune-constructing wind regimes, or the long-term winds, are particularly useful to facilitate atmospheric modeling, such as in General Circulation Models (GCMs). Still, the recent near-surface wind regimes may facilitate a better understanding of current climate and atmospheric conditions, so they may have potential to provide atmospheric modeling with a new temporal and spatial scale for near-surface wind constraints. This project also encourages future studies on a comparison of long-term and short-term wind regimes and their implications for climate.

6. Conclusions

HiRISE images provide the capability to examine small-scale aeolian deposits, such as sand ripples, on Mars. In this study, we established a systematic mapping procedure for ripples on small sand dunes to reveal near-surface wind patterns. We chose three nearby sand dune fields on the floors of craters west of Hellas Basin, then produced surface process and flow maps based on documented ripple orientation and dune morphology. The mapping results show (1) the complexity of surface wind patterns, (2) the likely local occurrence of form–flow interactions, and (3) the possible persistence of NE and ESE winds during the past thousands of years. The near-surface wind directions inferred from ripple orientation provide a 'snapshot' of the recent wind regime. The mapping procedure developed in this study validates the feasibility and utility of mapping ripples and sand dunes on Mars, which encourages the use of this technique to study ripples and wind patterns in other regions on Mars. By increasing the number of places where near-surface wind patterns have been documented globally, future results may impact both the understanding of sand deposits on Mars, and the relative roles and rates of sand mobility on both Mars and Earth, as well as improve our understanding of when and where form flow interactions may be important on Mars.

Acknowledgments

This project was carried out while Z.Y.-C.L. visited the National Air and Space Museum during the summers of 2013 and 2014, supported by funds from NASA MDAP Grant NNX12AJ38G. We would like to thank Jani Radebaugh and Eric Christiansen for their discussion and encouragement, and Molly Johnson for her technical support during the use of HiRISE images and ArcGIS. Nathan Bridges and Lori Fenton provided valuable suggestions and constructive reviews, which significantly improved the final manuscript.

References

Anderson, F.S. et al., 1999. Assessing the martian surface distribution of aeolian sand using a Mars general circulation model. J. Geophys. Res.: Planets 104 (E8), 18991–19002. http://dx.doi.org/10.1029/1999JE900024.

Bagnold, R.A., 1941. The Physics of Blown Sand and Desert Dunes. Chapman and Hall, London, 265p.

Bishop, M.A., 2011. Aeolian scours as putative signatures of wind erosion and sediment transport direction on Mars. Geomorphology 125 (4), 569–574. http://dx.doi.org/10.1016/j.geomorph.2010.10.029.

Bourke, M.C. et al., 2010. Extraterrestrial dunes: An introduction to the special issue on planetary dune systems. Geomorphology 121 (1), 1–14. http://dx.doi.org/10.1016/j.geomorph.2010.04.007.

Bridges, N.T. et al., 2007. Windy Mars: A dynamic planet as seen by the HiRISE camera. Geophys. Res. Lett. 34 (23). http://dx.doi.org/10.1029/2007GL031445.

Bridges, N.T. et al., 2010. Aeolian bedforms, yardangs, and indurated surfaces in the Tharsis Montes as seen by the HiRISE Camera: Evidence for dust aggregates. Icarus 205 (1), 165–182. http://dx.doi.org/10.1016/j.icarus.2009.05.017.

Bridges, N.T. et al., 2011. Planet-wide sand movement on Mars as documented by the HiRISE camera. Lunar Planet. Sci. 42, 1215.

Bridges, N.T. et al., 2012a. Planet-wide sand motion on Mars. Geology 40 (1), 31–34. http://dx.doi.org/10.1130/G32373.1.

Bridges, N.T. et al., 2012b. Earth-like sand fluxes on Mars. Nature 485 (7398), 339–342. http://dx.doi.org/10.1038/nature11022.

Bridges, N. et al., 2013. Bedform migration on Mars: Current results and future plans. Aeolian Res. 9, 133–151. http://dx.doi.org/10.1016/j.aeolia.2013.02.004.

Chojnacki, M. et al., 2011. Orbital observations of contemporary dune activity in Endeavor crater, Meridiani Planum, Mars. J. Geophys. Res.: Planets 116 (E7), E00F19. http://dx.doi.org/10.1029/2010JE003675.

Christensen, P.R. et al., 2003. Morphology and composition of the surface of Mars: Mars Odyssey THEMIS results. Science 300 (5628), 2056–2061. http://dx.doi.org/10.1126/science.1080885.

Claudin, P., Andreotti, B., 2006. A scaling law for aeolian dunes on Mars, Venus, Earth, and for subaqueous ripples. Earth Planet. Sci. Lett. 252 (1), 30–44. http://dx.doi.org/10.1016/j.epsl.2006.09.004.

Durán, O., Claudin, P., Andreotti, B., 2011. On aeolian transport: Grain-scale interactions, dynamical mechanisms and scaling laws. Aeolian Res. 3 (3), 243–270. http://dx.doi.org/10.1016/j.aeolia.2011.07.006.

Edgett, K.S., Malin, M.C., 2000. New views of Mars eolian activity, materials, and surface properties: Three vignettes from the Mars Global Surveyor Mars Orbiter Camera. J. Geophys. Res.: Planets 105 (E1), 1623–1650. http://dx.doi.org/10.1029/1999JE001152.

Ewing, R.C. et al., 2010. Dune field pattern formation and recent transporting winds in the Olympia Undae Dune Field, north polar region of Mars. J. Geophys. Res.: Planets 115 (E8). http://dx.doi.org/10.1029/2009JE003526.

Fenton, L.K., Richardson, M.I., 2001. Martian surface winds: Insensitivity to orbital changes and implications for aeolian processes. J. Geophys. Res.: Planets 106 (E12), 32885–32902. http://dx.doi.org/10.1029/2000JE001407.

Fenton, L.K., Bandfield, J.L., Ward, A., 2003. Aeolian processes in Proctor Crater on Mars: Sedimentary history as analyzed from multiple data sets. J. Geophys. Res.: Planets 108 (E12). http://dx.doi.org/10.1029/2002JE002015.

Fenton, L.K. et al., 2014. Inverse maximum gross bedform-normal transport 2: Application to a dune field in Ganges Chasma, Mars and comparison with HiRISE repeat imagery and MRAMS. Icarus 230, 47–63. http://dx.doi.org/10.1016/j.icarus.2013.07.009.

Forget, F. et al., 2006. Formation of glaciers on Mars by atmospheric precipitation at high obliquity. Science 311 (5759), 368–371. http://dx.doi.org/10.1126/science.1120335.

French, R.G., Gierasch, P.J., 1979. The martian polar vortex: Theory of seasonal variation and observations of eolian features. J. Geophys. Res.: Solid Earth 84 (B9), 4634–4642. http://dx.doi.org/10.1029/JB084iB09p04634.

Gardin, E. et al., 2012. Dune fields on Mars: Recorders of a climate change? Planet. Space Sci. 60 (1), 314–321. http://dx.doi.org/10.1016/j.pss.2011.10.004.

Golombek, M. et al., 2010. Constraints on ripple migration at Meridiani Planum from Opportunity and HiRISE observations of fresh craters. J. Geophys. Res.: Planets 115 (E7), 2010. http://dx.doi.org/10.1029/2010JE003628.

Greeley, R., Iversen, J.D., 1985. Wind as a geological process on Earth, Mars, Venus and Titan. Cambridge Planetary Science Series.

Greeley, R. et al., 1992. Martian aeolian processes, sediments, and features. Mars 1, 730–766.

Greeley, R., Skypeck, A., Pollack, J.B., 1993. Martian aeolian features and deposits: Comparisons with general circulation model results. J. Geophys. Res.: Planets 98 (E2), 3183–3196. http://dx.doi.org/10.1029/92JE02580.

Greeley, R. et al., 2003. Wind-related features in Gusev crater, Mars. J. Geophys. Res.: Planets 108 (E12). http://dx.doi.org/10.1029/2002JE002006.

Greeley, R. et al., 2004. Wind-related processes detected by the Spirit rover at Gusev Crater, Mars. Science 305 (5685), 810–813. http://dx.doi.org/10.1126/science.1100108.

Hansen, C.J. et al., 2010. HiRISE observations of gas sublimation-driven activity in Mars' southern polar regions: I. Erosion of the surface. Icarus 205 (1), 283–295. http://dx.doi.org/10.1016/j.icarus.2009.07.021.

Hansen, C.J. et al., 2011. Seasonal erosion and restoration of Mars' northern polar dunes. Science 331 (6017), 575–578. http://dx.doi.org/10.1126/science.1197636.

Haberle, R.M., Murphy, J.R., Schaeffer, J., 2003. Orbital change experiments with a Mars general circulation model. Icarus 161 (1), 66–89. http://dx.doi.org/10.1016/S0019-1035(02)00017-9.

Hayward, R.K. et al., 2007. Mars global digital dune database and initial science results. J. Geophys. Res.: Planets 112 (E11). http://dx.doi.org/10.1029/2007JE002943.

Hayward, R.K. et al., 2009. Aeolian dunes as ground truth for atmospheric modeling on Mars. J. Geophys. Res.: Planets 114 (E11). http://dx.doi.org/10.1029/2009JE003428.

Hayward, R.K., Fenton, L.K., Titus, T.N., 2014. Mars Global Digital Dune Database (MGD^3): Global dune distribution and wind pattern observations. Icarus 230, 38–46. http://dx.doi.org/10.1016/j.icarus.2013.04.011.

Hersen, P., Douady, S., Andreotti, B., 2002. Relevant length scale of barchan dunes. Phys. Rev. Lett. 89 (26), 264301. http://dx.doi.org/10.1103/PhysRevLett.89.264301.

Howard, A.D., 1977. Effect of slope on the threshold of motion and its application to orientation of wind ripples. Geol. Soc. Am. Bull. 88 (6), 853–856.
Howard, A.D., 1980. Effect of wind on scarp evolution on the martian poles. Rep. Planet. Geol. Prog. 1, 333–335.
Hugenholtz, C.H., Wolfe, S.A., 2009. Form–flow interactions of an aeolian saucer blowout. Earth Surf. Proc. Land. 34 (7), 919–928. http://dx.doi.org/10.1002/esp.1776.
Hunter, R.E., 1977. Basic types of stratification in small eolian dunes. Sedimentology 24 (3), 361–387. http://dx.doi.org/10.1111/j.13653091.1977.tb00128.x.
Johnson, M., Zimbelman, J.R., 2013. Characterization of small sand dunes on Mars. Lunar Planet. Sci. 44. Abstract 2111.
Johnson, M., Zimbelman, J.R., 2014. Documentation of sand ripple patterns and recent surface winds on martian dunes. Lunar Planet. Sci. 45. Abstract 1518.
Johnson, M.B., Zimbelman, J.R., 2015. Ripple orientations as an indication of recent winds on martian dunes. Lunar Planet. Sci. 46, Abstract 1539.
Kieffer, H.H., Christensen, P.R., Titus, T.N., 2006. CO_2 jets formed by sublimation beneath translucent slab ice in Mars' seasonal south polar ice cap. Nature 442 (7104), 793–796. http://dx.doi.org/10.1038/nature04945.
Kok, J.F., 2010. Difference in the wind speeds required for initiation versus continuation of sand transport on Mars: Implications for dunes and dust storms. Phys. Rev. Lett. 104 (7), 074502. http://dx.doi.org/10.1103/PhysRevLett.104.074502.
Kok, J.F. et al., 2012. The physics of wind-blown sand and dust. Rep. Prog. Phys. 75, 106901, http://iopscience.iop.org/0034-4885/75/10/106901.
McEwen, A.S. et al., 2007. Mars reconnaissance orbiter's High Resolution Imaging Science Experiment (HiRISE). J. Geophys. Res.: Planets 112 (E5). http://dx.doi.org/10.1029/2005JE002605.
McEwen, A.S. et al., 2010. The High Resolution Imaging Science Experiment (HiRISE) during MRO's primary science phase (PSP). Icarus 205 (1), 2–37. http://dx.doi.org/10.1016/j.icarus.2009.04.023.
Nielson, J., Kocurek, G., 1987. Surface processes, deposits, and development of star dunes: Dumont dune field, California. Geol. Soc. Am. Bull. 99 (2), 177–186.
Parteli, E.J. et al., 2009. Dune formation under bimodal winds. Proc. Natl. Acad. Sci. USA 106 (52), 22085–22089.
Piqueux, S., Christensen, P.R., 2008. North and south subice gas flow and venting of the seasonal caps of Mars: A major geomorphological agent. J. Geophys. Res.: Planets 113 (E6). http://dx.doi.org/10.1029/2007JE003009.
Pollack, J.B. et al., 1990. Simulations of the general circulation of the martian atmosphere: 1. Polar processes. J. Geophys. Res. 95 (B2), 1447–1473. http://dx.doi.org/10.1029/JB095iB02p01447.
Reffet, E. et al., 2010. Formation and stability of transverse and longitudinal sand dunes. Geology 38 (6), 491–494.
Rubin, D.M., Hunter, R.E., 1987. Bedform alignment in directionally varying flows. Science 237 (4812), 276–278.
Rubin, D.M., Ikeda, H., 1990. Flume experiments on the alignment of transverse, oblique, and longitudinal dunes in directionally varying flows. Sedimentology 37 (4), 673–684.
Sharp, R.P., 1963. Wind ripples. J. Geol. 71, 617–636. http://dx.doi.org/10.1111/j.1365-3091.1990.tb00628.x.
Silvestro, S. et al., 2010. Ripple migration and dune activity on Mars: Evidence for dynamic wind processes. Geophys. Res. Lett. 37 (20). http://dx.doi.org/10.1029/2010GL044743.
Sullivan, R. et al., 2008. Wind-driven particle mobility on Mars: Insights from Mars Exploration Rover observations at "El Dorado" and surroundings at Gusev Crater. J. Geophys. Res. 113 (E6). http://dx.doi.org/10.1029/2008JE003101.
Thomas, P., 1981. North–south asymmetry of eolian features in martian polar regions: Analysis based on crater-related wind markers. Icarus 48 (1), 76–90.
Thomas, P., Veverka, J., Campos-Marquetti, R., 1979. Frost streaks in the south polar cap of Mars. J. Geophys. Res. 84 (B9), 4621–4633.
Walker, I.J., Nickling, W.G., 2002. Dynamics of secondary airflow and sediment transport over and in the lee of transverse dunes. Prog. Phys. Geogr. 26 (1), 47–75.
White, B.R., 1979. Soil transport by winds on Mars. J. Geophys. Res. 84, 4643–4651.
Wilson, I., 1972. Sand waves. New Sci. 53, 634–637.
Wilson, S.A., Zimbelman, J.R., 2004. Latitude-dependent nature and physical characteristics of transverse aeolian ridges on Mars. J. Geophys. Res.: Planets 109 (E10). http://dx.doi.org/10.1029/2004JE002247.
Zimbelman, J.R., 2003. Decameter-scale Ripple-like features in Nirgal Vallis as revealed in THEMIS and MOC imaging data. In: Sixth International Conference on Mars, vol. 1, p. 3028.
Zimbelman, J.R., 2010. Transverse aeolian ridges on Mars: First results from HiRISE images. Geomorphology 121 (1), 22–29. http://dx.doi.org/10.1016/j.geomorph.2009.05.012.